



Eu based layered EuFAgX (X = S, Se and Te) magnetic semiconductors for optoelectronic and thermoelectric applications

Hessa Al Salmah¹ · Shahid Mehmood²

Received: 21 July 2023 / Accepted: 11 October 2023 / Published online: 10 November 2023

© The Author(s), under exclusive licence to Springer Science+Business Media, LLC, part of Springer Nature 2023

Abstract

Structural, optoelectronic, thermoelectric and magnetic properties of layered structured compounds EuFAgX (X = S, Se and Te) are investigated using density functional theory (DFT). Structural properties are in good agreement with the reported outcomes. Electronic properties shows that the understudy compounds are visible light active direct bandgap semiconductors. Electrical conductivity also reveals the semiconducting nature of these compounds. This study reveals that the substitution of Te by S causes reduction in band gape. The outcome demonstrates that EuFAgB (B = S, Se and Te) compounds are optically dynamic in the visible region and suitable for optoelectronic devices and are active aspirants for solar cell applications. Based on their thermoelectric characteristics, they are effective thermoelectric materials for thermoelectric power production for variable systems, nano-thermocouples and thermoelectric generation. Understudy compounds are A-type anti-ferromagnetic, as shown by magnetic susceptibility and magnetic ground state energy. Magnetic probes cannot read anti-ferromagnetic moments because of their anti-ferromagnetic structure, and data is unaffected by magnetic fields. Therefore, these compounds may be excellent candidates for magnetic cloaking devices.

Keywords Layered chalcogenides · First principal calculations · Optoelectronic properties · Thermal and magnetic properties · Solar cell application

✉ Shahid Mehmood
shahiduom07@gmail.com

Hessa Al Salmah
haALSALMA@imamu.edu.sa

¹ Department of Physics, College of Science, Imam Muhammad Ibn Saud Islamic University (IMSIU), 11623 Riyadh, Saudi Arabia

² Department of Physics, University of Malakand, Chakdara, Dir (Lower) 18800, Pakistan

1 Introduction

Research into fluorine based compounds (Shahzad et al. 2023) is ongoing and extensive. They are of such intense interest because even their most fundamental crystalline structure exhibits a wide variety of catalytic, optical, electric, magnetic, magneto-resistive and piezoelectric properties (Bouafia et al. 2015; Rehman et al. 2021). Due to their inherent superlattice properties like nearly two-dimensional electronic structures, the fluoro-chalcogenides have gained a lot of interest (Yanagi et al. 2003, 2006; Zou et al. 2016, 2013; Ul Islam et al. 2017; Gudelli et al. 2015; Charkin et al. 2014, 2012; Richard et al. 2012; Liu et al. 2016; Bannikov et al. 2012a, 2012b; Zakutayev et al. 2010a, 2010b, 2010c, 2011; Bannikov and Shein 2010; Pottgen and Johrendt 2008; Park et al. 2007; Yasukawa et al. 2004; Boudiaf et al. 2017a; Wager et al. 2008; Hiramatsu et al. 2007). They show promise as components in a variety of cutting-edge technologies, including p-type semiconductors (Yanagi et al. 2003; Zakutayev et al. 2010b; Pottgen and Johrendt 2008; Wager et al. 2008), thermoelectric (Zou et al. 2016, 2013; Gudelli et al. 2015; Yasukawa et al. 2004), optoelectronic devices (Zou et al. 2016; Hiramatsu et al. 2007) and photovoltaic (Zakutayev et al. 2010b, 2011).

These compounds adopted the structure of LaOAgS, also known as "1111" structure and composed of two groups (Charkin et al. 2012; Bannikov and Shein 2010). The superconductivity and magnetic properties of the metallic-like phases found in first group (Kamihara et al. 2008; Johnston 2010). The second group comprises the semiconducting 1111-like systems, which display unique optical properties (Bannikov and Shein 2010; Ueda et al. 2004; Kamioka et al. 2005). The 1111-like materials exhibit remarkable adaptability to a wide range of building blocks. The 1111-like oxy-chalcogenides have been the focus of most studies, but the 1111-like chalcogenide fluorides have received considerably less attention (Richard et al. 2012; Zou et al. 2013; Liu et al. 2016; Bannikov et al. 2012b).

Charkin et al. (Charkin et al. 2012) have recently synthesized the 1111 type fluoro-chalcogenides Sr/BaAgChF (Ch=S and Se) and studied extensively due to their photovoltaic application (Boudiaf et al. 2017a, 2018). It is evident from the EuAg₄Pn₂ pnictides (Pn=As and Sb) (Gerke et al. 2013) implies that the arrangement of Eu²⁺ and Ag⁺ may be stable in certain crystal. Since the ionic radii of Eu²⁺ and Sr²⁺ are so near (1.17 and 1.18 Å (Shannon 1976), it is reasonable to assume that the EuFAgCh analogs of the previously obtained SrFAgCh (Ch=S, Se, and Te) compounds (Charkin et al. 2012) can likewise be prepared. Out of the three expected EuFAgCh compounds, only two were synthesized (Plokhikh et al. 2020) and their optical gaps are reported in the range of 2.11 and 2.26 eV respectively.

It is reported that these chalcogenides are active photovoltaic materials and the replacement of Eu by Sr enhances the optoelectronic and thermoelectric properties (Motomitsu et al. 2006; Hoat 2019; Hoat et al. 2019; Lin et al. 2020). It is evident that Eu play a significant role in the enhancement of the physical properties of these layered compounds, therefore in the current study the structural, optoelectronic, magnetic and thermoelectric properties of EuFAgX (X=S, Se and Te) compounds are estimated using density functional theory for thermoelectric and photovoltaic applications.

2 Computational detail

The full-potential linear augmented plane wave (FP-LAPW) approaches are used to execute the structure and optoelectronic nature of EuFAgX (X=S, Se and Te) inside a density functional theory (DFT) (Hohenberg and Kohn 1964) that is implemented in the WIEN2k

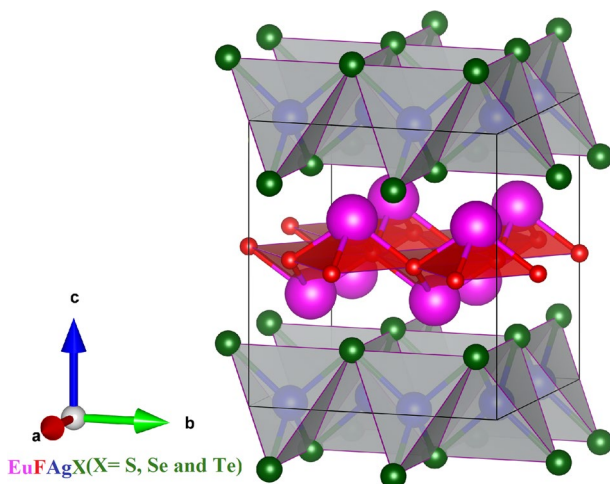
package (Blaha et al. 2020). Generalized Gradient Approximation (GGA-PBESol) (Perdew et al. 1996), GGA with Hubbard U (GGA + U) (Kohn and Sham 1965) are employed to treat the exchange and correlation while Becke-Johnson and modified Becke-Johnson potential (BJ and mBJ) (Tran and Blaha 2009; Koller et al. 2012) with Hubbard U (BJ/mBJ + U) With $J_{\text{eff}} = U - J$ was calculated treated by the method used by Tsuneda and Hirao (2014) using the self-interaction corrections (SIC) method by taking $J = 0$. Several values of Hubbard U were evaluated to optimize Hubbard U and $U = 7$ eV/Eu was selected for the current computations (Elqahtani et al. 2020; Taha et al. 2023) were also used for better treatment at very low computational rate. To prevent the outflow of charges, the FP-LAPW approach divides the area into an interstitial zone and a muffin-tin sphere region. In a muffin-tin sphere, a harmonic expansion setup is located close to around $l_{\text{Max}} = 10$ and is also set $R_{\text{MT}} = 1.0 / K_{\text{MAX}}$. Although a particular thousands number of K-points are used in the Brillouin Zone, the energy between subsequent iterations is assumed to be 0.1 mRy, and the force is lowered to 1 mRy Bohr⁻¹. Kramar Kroneg relation is used to estimate the optical properties and BoltzTrap package is used to estimates the temperature dependent properties (Madsen et al. 2006).

3 Results and discussion

3.1 Structural properties

The structural properties of these EuFagX (X = S, Se and Te) compounds are investigated employing experimentally reported structure data (Plokhikh et al. 2020) depicted in Fig. 1. The Birch-Murnaghan equation of state (Birch 1947) is set to evaluate the unit cell of each compound through the GGA + U shown in Fig. 2 to determine the structure properties and the detail of which are provided in Table 1. The lattice constants from the Table 1 are $a = b = 4.05$ Å and $c = 9.23$ Å for EuFagS, $a = b = 4.14$ Å and $c = 9.20$ Å for EuFagSe and $a = b = 4.30$ Å and $c = 9.52$ Å for EuFagTe. The results reported for these compounds are relatively close to experimental results (Plokhikh et al. 2020) and are increasing when X goes from S to Te due to increasing in their atomic radii and

Fig. 1 Unite cell structure of layered structured EuFagX (X = S, Se and Te) compounds



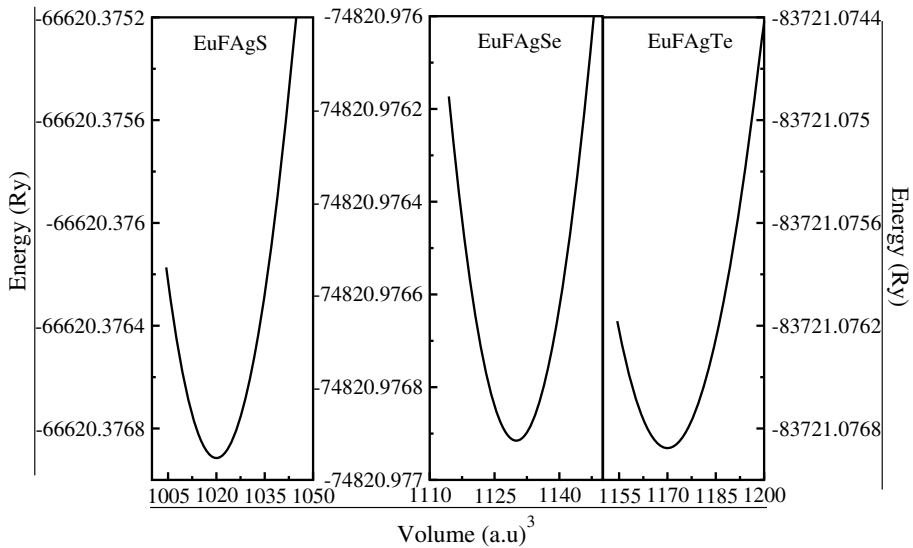


Fig. 2 Energy versus volume optimization curve of the layered structured EuFAgX (X=S, Se and Te) compounds

larger than the isotropic compound BaMnPnF (Pn=As, Sb, Bi) (Plokhikh et al. 1111; Saparov et al. 2013), EuFZnPn (Pn=P, As, Sb) (Plokhikh et al. 2016) and comparable with the others silver based compounds (BiAgOCh; Ch=S, Se or Te and BaAgFCh (Ch=S, Se or Te)) (Gamon et al. 2018; Boudiaf et al. 2017b). The computed bulk moduli (B_0) of the understudy compounds are of 83.28, 94.98 and 121.33 GPa respectively.

Table 1 Calculated lattice constants, bulk modulus, ground state energy, bond lengths and bond angles of the EuFAgX (X=S, Se and Te) compounds

Parameters	EuFAgS	EuFAgSe	Exp(Plokhikh et al. 2020)	EuFAgTe	Exp(Plokhikh et al. 2020)
a (Å)	4.05	4.14	4.15	4.31	4.32
c (Å)	9.23	9.20	9.21	9.53	9.54
c/a	2.27	2.21	–	2.21	–
B_0 (GPa)	83.28	94.98	–	121.33	–
E_0 (Ry)	–66,620.37689	–74,820.97695	–	–83,721.0770	–
E_{Coh} (Ry)	–2.1779	–3.3267	–	–5.0852	–
ΔH (Ry)	–0.5444	–0.8316	–	–1.2713	–
Eu-F	2.46	2.49	2.50	2.52	2.54
Eu-B	3.15	2.24	3.25	3.41	3.42
Ag-B	2.66	2.74	2.75	2.86	2.88
θ_1 (Eu-F-Eu)deg	106.89	110.97	111.85	114.78	115.87
θ_2 (Eu-F-Eu)deg	114.12	107.67	108.29	97.11	97.30
θ_1 (B-Ag-B)deg	92.87	96.87	97.73	104.56	105.96
θ_2 (B-Ag-B)deg	119.54	115.26	115.64	112.87	116.75

B_0 for EuFAgTe is larger than the rest compounds confirms that this compound is harder among the series.

The theoretical stability parameter cohesive energy (E_{Coh}) and enthalpy of formation (ΔH) has been determined (Plokhikh et al. 2020) from E_0 and is listed in Table 1. Coulomb interactions flanked by nuclei and electrons in a compound lead to more incredible E_{Coh} and ΔH , indicating the system is tightly coupled and integrated. As the electron-nucleus interaction energy increases, the system becomes more tightly coupled. The E_{Coh} and ΔH of EuFAgX (X = S, Se and Te) compounds lie in the range of -5.0852 to -2.1779 Ry and -1.2713 to -0.5444 Ry respectively. The negative values of E_{Coh} and ΔH shown in Table 1 demonstrate their thermodynamic stability. According to E_{Coh} and ΔH EuFAgTe is the most stable compound and is due to the higher value than the of EuF-AgX (X = S and Se).

The calculated bond lengths between the Eu-F, Eu-X and Ag-X and bond angles θ_1 and θ_2 .

between Eu-F-E and θ_1 and θ_2 between X-Ag-X at different site in comparison with the experimental results of available compounds are listed in Table 1. The reported data are in agreement with the experiments as clear from the Table 1 (Plokhikh et al. 2020) and show that bond length between the Eu-F, Eu-X and Ag-X are varying in the range of 2.46 to 2.52 Å, 3.15 to 3.41 Å and 2.66 to 2.86 Å respectively for the compounds EuFAgX (X = S, Se and Te) and bond angle θ_1 between the Eu-F-Eu and θ_1 between X-Ag-X are changing from 106.89 to 114.78 and 92.87 to 104.56(°) respectively for the compounds EuFAgX (X = S, Se and Te) and bond angle θ_2 between the Eu-F-Eu and X-Ag-X are changing from 114.12 to 97.11(°) and 119.54 to 112.87(°) respectively for these compounds. Similarly the Bi-O-Bi angles in BiCuSeO and BiCuTeO lie in the range of 105.10°-118.60° while for AgBiTeO is 90.01° to 119.99° which show that these compounds are less distorted than the ABiTeO (Mukherjee and Singh 2020), and have more distortion in the structure as compare to BiCuSeO and BiCuTeO (Hiramatsu et al. 2008).

As seen in the different plan view of Fig. 1 these compounds are made up of $[\text{Eu}_2\text{F}_2]^{2+}$ cationic fluorite-type blocks and $[\text{Ag}_2\text{X}_2]^{2-}$ (X = S-Te) anionic layers that are indefinitely extended along the 4-axis. Additionally, each FEu_4 tetrahedral block is encircled by AgB_4 tetrahedral block. One Eu and four F atoms make up the FEu_4 block (Fig. 1). The c/a ratio shows how the tetrahedra is flattened. If c/a ratio is small the tetrahedra will be more flattened and hence the Eu-F-Eu angle will be large. In Table 1 it is shown that as we go from S to Te base compounds the c/a ratio decreases and θ_1 between Eu-F-Eu and X-Ag-X increases. As the θ_1 increases causes to reduce the θ_2 between Eu-F-Eu and X-Ag-X in EuFAgX (X = S, Se and Te) compounds.

On the other hand the small dissimilarity in the ionic radii of Sr and Eu make it clear that the cell structures of the studied compounds are extremely close to the equivalent strontium based fluoride chalcogenides (Shannon 1976). Very comparable bonding patterns are reflected in the nearly identical Ag-B bond distance in the Sr, Ba and Eu based compounds. Because of the growing mismatch between the FN_4 (N = Eu, Sr or Ba) and CX_4 (C = Cu, or Ag) tetrahedra, the N-F distances elongate significantly and exhibit very similar increase upon replacing S with Se and Se with Te. The pattern is indistinguishable from that illustrated for iso-structural Mg, Mn, Zn, and Cd pnictides (Charkin et al. 2012; Birch 1947; Plokhikh et al. 1111, 2018; Saparov et al. 2013). There is a correspondence between the N-X distances of Cu and Ag compounds and the Eu-Te distances of the structurally related $\text{Cu}_{0.66}\text{EuTe}_2$ (Patschke et al. 1999).

3.2 Electronic properties

The number of states occupied by a system at any energy is described by its density of states, and this function determines the bulk characteristics of materials. The total density of states (TDOS) for the compounds under investigation is calculated using GGA-PBESol, GGA+U, BJ+U and mBJ+U approaches and presented in Fig. 3. The TDOS for these compounds reveals the presence of energy gap flanked by the conduction bands (CB) and valance band (VB) and there is no overlapping of densities around the Fermi level (E_F) disclose the semiconductor nature of EuFAGX (X=S, Se and Te) compounds through GGA+U, BJ+U and mBJ+U while shows metallic nature via GGA potential. As these compounds are reported semiconductor therefore the results calculated by GGA potential is unacceptable while estimated results through GGA+U, BJ+U and mBJ+U is reasonable due to in agreement with the experimental results additionally the electron possessed by Eu-f states are strongly correlated and cannot be treated by GGA potential.

From the TDOS the estimated bandgap values are given in Table 2. The estimated bandgaps are 2.10 eV, 2.27 eV and 3.51 eV for EuFAGS, 1.98 eV, 2.07 eV and 3.20 eV for EuFAGSe and 1.77 eV, 1.99 and 2.96 eV for EuFAGTe by GGA+U, BJ+U and mBJ+U potentials. The reported bandgap for EuFAGS is 2 eV to 2.22 eV, for EuFAGSe is 1.71 eV and 2.11 eV and for EuFAGTe is 1.95 eV and 2.26 eV by Plokhikh et al. (Plokhikh et al. 2020). In the current study different potentials were used to find out the correct and exact nature of bandgap value for these compounds. According to reported band gaps, the investigation through BJ+U is reasonable (Plokhikh et al. 2020). Therefore, all the other properties are estimated by employing BJ+U potential.

Similarly the chalcogenides BaFAGCh (Ch=S, Se and Te) are also direct band gap semiconductors and their band gap values obtained through TB-mBJ (GGA-08) is 2.81 eV

Fig. 3 Total DOS of the layered structured EuFAGX (X=S, Se and Te) compounds

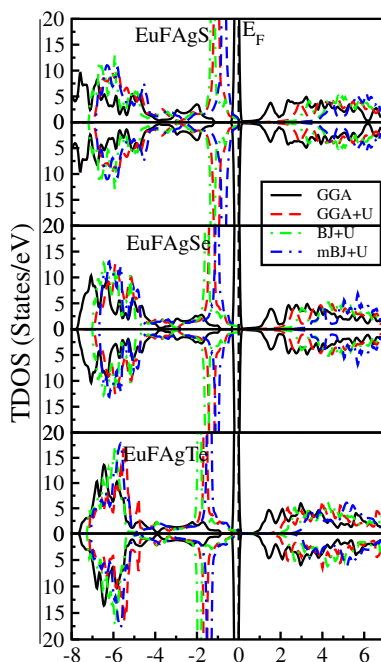


Table 2 Comparison of present and others band gaps of the EuFAgX (X = S, Se and Te) compounds

Compounds	GGA	GGA + U	BJ + U	mBJ + U	Other(Plokhikh et al. 2020)	Exp(Plokhikh et al. 2020)
EuFAgS	Metal	2.10	2.27	3.51	2.0	2 to 2.22
EuFAgSe	Metal	1.98	2.07	3.20	1.71	2.11
EuFAgTe	Metal	1.77	1.90	2.96	1.95	2.26
Eu/ μ_B FAgS	6.97	7.87	–	–	–	–
Eu/ μ_B FAgSe	6.94	7.69	–	–	–	7.78
Eu/ μ_B FAgTe	6.91	7.56	–	–	–	7.45

(1.451 eV) for BaFAgS, 2.66 eV (1.32 eV) for BaFAgSe and 2.59 eV (1.53 eV) for BaF-AgTe (Boudiaf et al. 2017b). The band gap value of SrCuFS is 3.0 eV and SrCuFSe is 2.7 eV (Shannon 1976); BaCuFS is 3.2 eV and BaCuFSe is 3.0 eV; BaCuFTe is 2.3 eV (Park et al. 2007). The estimated band gap is 1.1 eV for BiCuOS and 0.8 eV for BiCuOSe and 0.4 for BiCuOTe (Hiramatsu et al. 2008). 3.1 eV for LaCuOS, 2.8 eV is for LaCuOSe and 2.4 eV is for LaCuOTe (Hiramatsu et al. 2008). These band gaps for the understudy compounds are much smaller than these isotropic compounds due to huge difference in the atomic radii of constituent's atoms. On the other hand there is a clearly isotropic trend in the decreasing of band gap as Ch goes from S to Te.

The figure also disclose that as we go from S to Te the band gap reduces for the under study compounds, because of increase in anion size or generally the band gap should be reduced when more electronegative cations are replaced with less electronegative ones, and this is indeed the case: going from 0.33 eV to 0.15 eV in the $Sr_3In_2As_4$ to $Eu_3In_2As_4$ (Taha et al. 2023) and also growing from GGA \rightarrow mBJ + U.

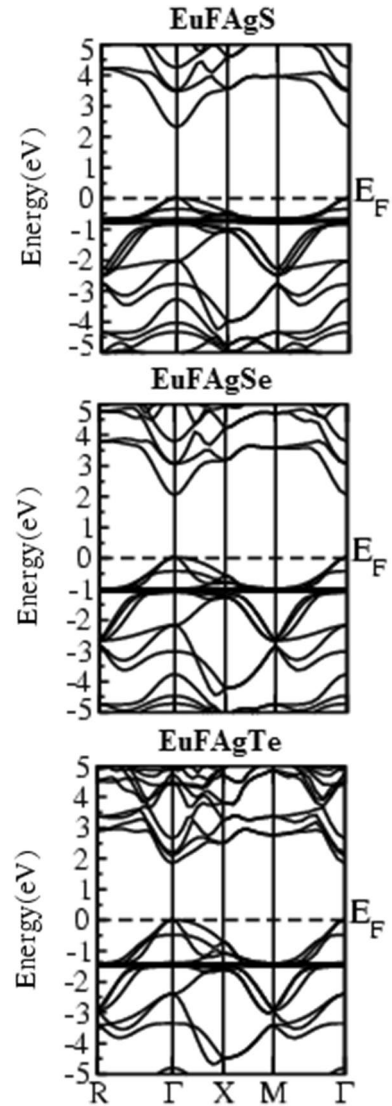
Additionally, the band structures for EuFAgX (X = S, Se and Te) are calculated and displayed in Fig. 4 to further validate their semiconducting nature. The figure shows that there is no overlapping at the E_F and maxima of VB align with the minima of CB at the central symmetry for both compounds indicate their direct band gap character.

The element's partial density of states (PDOS) is also considered to determine their relative importance, as shown in Fig. 5 demonstrates that densities are distributed in two sections in the whole energy range. Eu-f, F-p, Ag-d and B-p states take part in the section from -7.5 eV to 0 eV and from threshold value to 6.5 eV correspondingly in all compounds with variation in contributions in the VB and CB such that the contribution of B-p are greater than the Eu-f, Ag-d and F-p in CB as compare to VB while Eu-f state shows greater contribution in the VB as compare to CB. From the VB and CB, it is evident that their energy gap accure between the d state of Ag-d, B-p and B-P atom in all compounds. Additionally compared to other compounds of the same kind, such as the EuFZnPn and EuFMnPn series, the electronic structures of the EuFAgB series are in excellent agreement with these isotropic compounds.

3.3 Optical properties

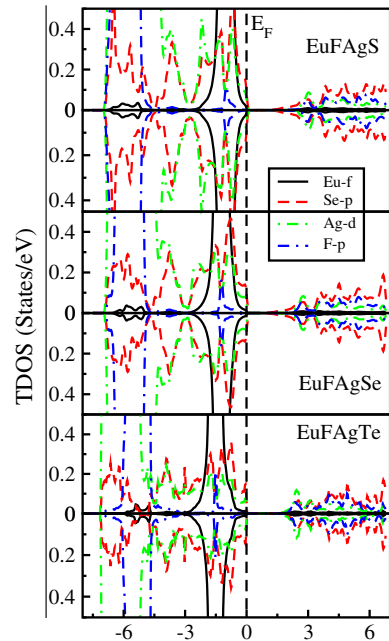
Optical properties of materials refer to how they interact with light, including how they absorb, reflect and transmit light. These properties play a crucial role in various applications, such as designing optical devices, understanding material behavior, and developing new technologies and play a crucial role in various technologies and industries, including

Fig. 4 Electronic band of the layered structured EuFAgX (X=S, Se and Te) compounds



electronics, photonics, optoelectronics and solar cells. Therefore it is significant to examine the interaction of light wave with these materials in response to the optoelectronic application. Thus, optical properties for the under study compounds EuFAgB (B=S, Se and Te) are estimated in the energy range of 0-14 eV. In the presented work the calculated optical factors are real and imaginary component of the dielectric function ($\epsilon_1(\omega)$ and $\epsilon_2(\omega)$), oscillator strength ($\sigma(\omega)$), extinction coefficient ($k(\omega)$), energy loss function ($L(\omega)$), reflectivity ($R(\omega)$) refractive index ($n(\omega)$), and optical conductivity ($\alpha(\omega)$) in the three (X and Z) axis and given in Fig. 6a-b. In Fig. 6a, the compound's various physical properties are represented by the real component of the $\epsilon_1(\omega)$. The static dielectric function ($\epsilon_1(0)$) is the value occur at the 0 frequency limit. In Fig. 6a the ($\epsilon_1(0)$) lie at 4.97 eV, 5.69 eV and 7.22 eV in X direction and 4.35, 4.76 and 5.87 eV in Z direction respectively for all

Fig. 5 Partial DOSs of the layered structured EuFAgX (X = S, Se and Te) compounds



EuFAgX (X = S, Se and Te) compounds. The value of $\epsilon_1(0)$ at X direction are 5.01, 5.92 and 7.46 and at Z direction the $\epsilon_1(0)$ is 4.35, 5.43 and 6.0 respectively. The $\epsilon_1(0)$ for the under study compounds are very close to BaFAgCh (Ch = S, Se and Te) and SrFCuCh (Ch = S, Se and Te) (Shannon 1976; Boudiaf et al. 2017b) such that the $\epsilon_1(0)$ for these compounds lies in the range of 4.625–6.294 and 4.70–5.472 respectively at X and Z directions. Spectra are seen to increase after the zero frequency, peak at their highest points are 6.86, 7.39 and 9.66 lies at 4.39 eV, 2.10 eV and 3.00 eV in X axis and 8.04, 8.60 and 10.84 lies at 4.50 eV, 4.34 eV and 3.49 eV in z axis respectively for EuFAgX (X = S, Se and Te) compounds. Additionally the $\epsilon_1(0)$ show inverse relation with the band gap and agree with the model presented by Penn et al. (Penn 1962) and the difference in the $\epsilon_1(0)$ at x and z axis indicate the optical anisotropy reveal by the under study compounds. The spectra are seen to decline and eventually drop to zero after this highest peak. The substance has lost its dielectric properties and has turned into metal (Hu et al. 2022; Selmani et al. 2022).

The $\epsilon_2(\omega)$ is provided in Fig. 6a associated with the absorption property of the materials and are zero up to the energies below the estimated band gap as indicate clearly that up to 1.97 eV and 2.02 eV, 1.84 eV and 1.92 eV, 1.56 eV and 1.74 eV there is no spectra which correspond to the optical gap of these compounds in x and z crystallographic axis respectively. The Figure also shows that the optical gap shrinks from S to Te due to increase in the lattice constants as also clear from the Figs. 3 and 4. The band gaps reported for these compounds are found active in visible region make them potential applicant for solar cell application.

The same trend as reduction in band gap is also observed in the isotropic BiAgOCh Ch = S and Se while BaFAgCh and SrFCuCh Ch = S, Se and Te) compounds (Motomitsu et al. 2006; Hoat 2019; Hoat et al. 2019; Gamon et al. 2018; Hiramatsu et al. 2008). In Fig. 6a After the threshold value the rise in the curve is apparent in compounds EuFAgX (X = S, Se and Te) on x-axis achieved the highest peak at 5.94 eV, 5.72 eV and 4.55 eV

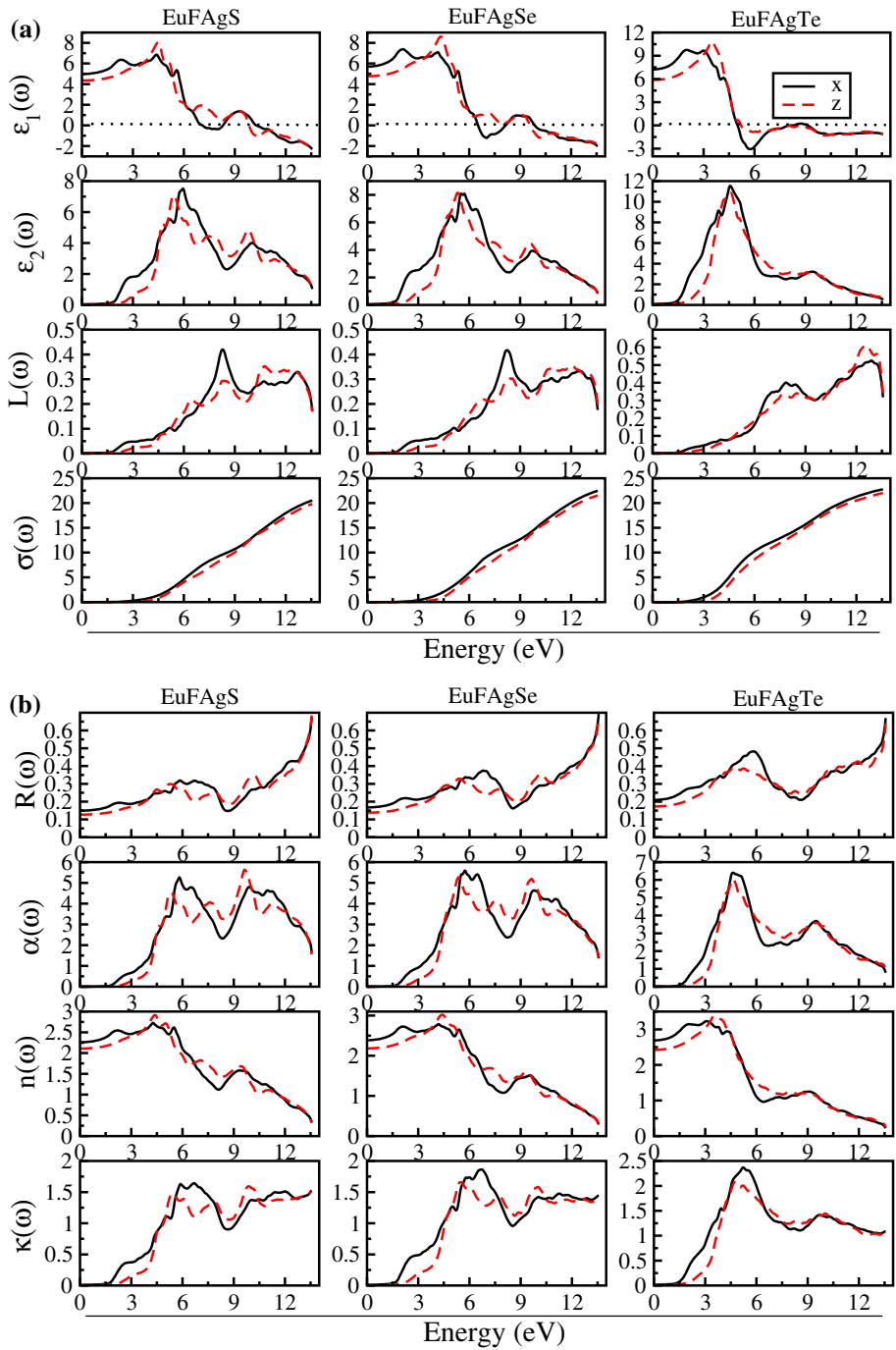


Fig. 6 (a, b) Optical plots of the layered structured EuFAgX (X=S, Se and Te) compounds

respectively and on z-axis achieved the highest peak at 5.40 eV, 5.31 eV and 4.58 eV respectively due to major inter bond transition (Almishal and Rashwan 2022; Rehman et al. 2022).

Figure 6a shows the reflectivity ($R(\omega)$) for the understudy compounds. According to the graph, the zero-energy reflectance ($R(\omega)$ at 0 eV ($R(0)$) for EuFAgX (X = S, Se and Te) are in the range of 14 to 21% on x-axis and 12 to 18% on z-axis respectively. Similarly BaFAgCh shows $R(0)$ up to 13 to 17% at x axis and 12 to 16% at z axis, SrFCuCh (Ch = S, Se and Te) shows 13.4 to 18.5% at x axis and 11.7 to 17.2% at z-axis respectively (Shannon 1976; Plokhikh et al. 2020; Motomitsu et al. 2006; Hoat 2019; Hoat et al. 2019). In comparison the understudy compounds are more reflective than Sr and Ba base chalcogenides at zero frequency limit. Highest reflectivities of 68 to 69% correspond to 13.56 eV for EuF-AgS on x and z-axis respectively, highest reflectivity of 70 to 67% correspond to 13.56 eV for EuFAgSe on x and z-axis respectively and highest reflectivity of 67 to 64% correspond to 13.56 eV for EuFAgTe on x and z-axis respectively. The maximum reflectivity shown by SrFCuCh (Ch = S, Se and Te) lie in the range of 39.56 to 45.5% and 33.89 to 36.80% at x and z axis in the ultraviolet region also demonstrate that the understudy compounds indicate greater reflectivity than the SrFCuCh (Ch = S, Se and Te) (Shannon 1976; Plokhikh et al. 2020; Motomitsu et al. 2006; Hoat 2019; Hoat et al. 2019). Curiously, reflectance increases as energy approach the point where $\epsilon_1(\omega)$ becomes zero. The high reflectivity in these materials occurs at ultraviolet region therefore high-frequency radiation might be blocked by using these materials and are more suitable than the isotropic SrFCuCh (Ch = S, Se and Te) (Shannon 1976; Plokhikh et al. 2020; Motomitsu et al. 2006; Hoat 2019; Hoat et al. 2019; Sharma et al. 2022; Su et al. 2022; Qaisi et al. 2022).

Figure 6b correspond to refractive index ($n(\omega)$). The fixed value of the refractive index ($n(0)$) is computed in the range 2.26 to 2.68 on x-axis and 2.10 to 2.42 on z-axis for EuF-AgX (X = S, Se and Te) respectively. The value of the $n(0)$ demonstrate that it follow the relation $(n(0) = \sqrt{\epsilon_1(0)})$ and are close to the $n(0)$ (2.15–2.33 and 2.05–2.13 at x and z axis) for SrFCuCh (Ch = S, Se and Te) (Shannon 1976; Plokhikh et al. 2020; Motomitsu et al. 2006; Hoat 2019; Hoat et al. 2019). After $n(0)$ real part of $n(\omega)$ rises and reach its peak value where the value of energies are 4.28 eV, 4.17 eV and 3.06 eV on x-axis and 4.99 eV, 4.42 eV and 3.52 eV on z-axis for EuFAgX (X = S, Se and Te) respectively. The prominent values of $n(\omega)$ observed for the compounds under investigation respectively is due to the drop off in the maximum number of photons upon entry to the materials (Khan et al. 2022).

$L(\omega)$ is the energy loss function for moving electrons inside a material is seen in Fig. 6a. The peak in the curve of the understudy compounds is caused by plasma frequency resonance. $L(\omega)$, which depends on loss of energy and momentum transfer (Ullah et al. 2016; Loughin et al. 1996), measures the material response to an electromagnetic perturbation. According to Fig. 6a, the lower energy related with photons than the bandgap value results in no scattering. Figure 6a shows that the presence of discrete energy bands causes the EuFAgX (X = S, Se and Te) compounds to loss energy at 8.28, 8.20 and 12.88 eV respectively on x-axis and loss energy at 8.34, 8.53 and 12.53 eV on z-axis respectively.

To quantify the quantity of electrons concerned in an optical transition, the oscillator strength ($\sigma(\omega)$) or sum rule is needed. The calculation of oscillator strength was done for current compounds which are under studies; Fig. 6a demonstrates when energy increase then $\sigma(\omega)$ also enhances. As the energy increases past the bandgap, the number of electrons in the system rapidly increases from zero when the energy is low. It is obvious from Fig. 6a that the $\sigma(\omega)$ demonstrates that 19–23 numbers of electron in both x and z axis

involve in the optical transition appropriately in different orientations of EuFAgX (X = S, Se and Te).

Electrons will conduct through the material when an electromagnetic field is produced, and optical conductivity is a crucial optical property for this to happen. The $(\alpha(\omega))$ spectra of these EuFAgX (X = S, Se and Te) compounds are displayed in Fig. 6b. According to Fig. 6b, optical conduction begins around the threshold value and continues to increase beyond it, reaching maximal conductivity of 5.25, 5.59 and 4.63 $\Omega^{-1} \text{ cm}^{-1}$ on x axis and 5.63, 5.18 and 6.05 $\Omega^{-1} \text{ cm}^{-1}$ on z axis for all EuFAgX (X = S, Se and Te) compounds respectively.

The extinction coefficient measure the relations of an electromagnetic wave with a material represented by $k(\omega)$ (Aliabad et al. 2009; Abasi et al. 2020; Al-Douri et al. 2012; Chaudhry et al. 2016; Benahmed et al. 2018; Salik et al. 2020). Accordingly, if a material's $k(\omega)$ is very small, it will have a small absorbance and a large transmittance. The extinction coefficient for little-studied chemicals is close to $\epsilon_2(\omega)$.

In Fig. 6b, it is apparent that mostly up to band gap the $k(\omega)$ have zero value and show little absorbance and high transmittance. The maximum value of 1.64 eV at 6.68 eV on x-axis and 1.59 eV at 9.86 eV on z-axis for EuFAgS, 1.86 eV at 6.70 eV on x-axis and 1.66 eV at 5.48 eV on z-axis for EuFAgSe and 1.54 eV at 3.93 eV on x-axis and 1.44 eV at 10.02 eV on z-axis for EuFAgTe respectively shows that in these region the compounds have poor wave transmission and strong wave absorption.

The optical properties show different responses in different crystallographic direction as clear from Fig. 6a, b and from Table 2 which demonstrate that these compounds are anisotropic optical materials and from the band gap value and optical conductivity these compounds are potential candidates for solar cell and photovoltaic applications.

3.4 Thermoelectric properties

The thermoelectric generator converts thermal energy to electrical power. As things go, the study explaining the thermoelectric (TE) properties is rapidly expanding. When thermoelectric materials are employed on a large scale (Computer cooling and TE refrigeration), their TE characteristics should be researched to evaluate their actual performance at relatively high temperatures. Active thermoelectric materials have been discovered in semiconductors with a narrow bandgap.

Transport parameters of these compounds are explored in a temperature from 25 to 800 K using the BoltzTrap program (Madsen et al. 2006). Electrical conductivity (σ) examines the flow of free charges. The estimated σ for EuFAgX (X = S, Se and Te) compounds is presented in Fig. 7. At lower temperatures, the σ for EuFAgX (X = S, Se and Te) are very low, while increasing with rises in temperature. Besides σ also increases as we go from S \rightarrow Te. The conductivity of the EuFAgTe is greater than the rest of two compounds because EuFAgTe possess low band gap as compare to EuFAgSe and EuFAgS. The variation in energy gap causes the alteration in electrical conductivity. At 300 K, the electrical conductivity of these compounds EuFAgX (X = S, Se and Te) 5.12×10^{17} , 6.14×10^{17} and 1.67×10^{18} S/ms respectively. Conversely the electrical conductivity of the Zn doped BiCu-SeO is 4.34×10^3 S/m, for Ca and Ba doped BiCuSeO are 20×10^3 S/m and 17.54×10^3 S/m respectively (Das et al. 2019; Zhao et al. 2014). The higher value of electrical conductivity for the understudy compounds are due to the involvement of the relaxation time and are comparable with the isotropic one.

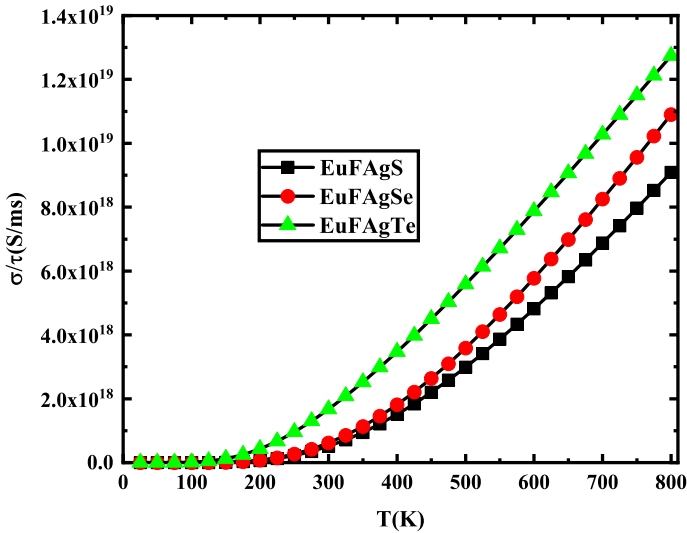


Fig. 7 Electrical conductivity of the layered structured EuFAgX (X=S, Se and Te) compounds

Lattice vibrations and electron conduction usually cause heat conduction in materials. Due to the BoltzTraP package's limitations, the electrical component of thermal conductivity (κ) for the understudied compounds is estimated, as given in Fig. 8. The κ increases substantially as the temperature rises, as shown in the graph. At low temperatures, the κ of the investigated compound are nearly constant, but they fluctuate as the temperature grows. The κ of these compounds are 3.91×10^8 , 1.37×10^9 and 2.79×10^9 W/mks at 300 K for EuFAgX (X=S, Se and Te) respectively. The κ for these compounds rises from EuFAgS to EuFAgSe and then to EuFAgTe.

The level of the thermoelectric voltage grows at the moment that two different materials are held at different temperatures. Limited voltage patterns result from temperature changes between two materials. When the temperature gradient is established, high thermoelectric voltage values verify increased degrees of efficiency. The efficiency of thermocouples is determined by the Seebeck coefficient (S), which determine the voltage ratio to the temperature differential.

Figure 9 shows the Seebeck coefficient (S) for EuFAgX (X=S, Se and Te) compounds. Positive value of S suggests a p-type semiconductor, while negative value indicates an n-type semiconductor. The value of S for these compounds are -1.71×10^{-5} , -2.97×10^{-5} and -4.38×10^{-5} V/K at 300 K respectively which shows its n-type semiconducting nature and reveals that electrons are principal carrier and S enhances with growing temperature for all these compounds.

The Seebeck coefficient values of BiCuSeO range from $350 \mu\text{VK}^{-1}$ at 300 K to $425 \mu\text{VK}^{-1}$ at 923 K, and decrease down to $69 \mu\text{VK}^{-1}$ at 300 K and $167 \mu\text{VK}^{-1}$ at 923 K upon 0.125 Ba.

doping (Zhao et al. 2014) and 286, 273 and 262 for Bi_{0.94}Zn_{0.06}CuSeO, Bi_{0.92}Zn_{0.08}CuSeO and Bi_{0.90}Zn_{0.10}CuSeO at 773 K respectively (Das et al. 2019). While from $55\text{--}178 \mu\text{VK}^{-1}$, for Bi_{1-x}Pb_xCuOTe (x=0, 0.01, 0.02, 0.04 and 0.06) at 300 K (An et al. 2014). The Seebeck value for the understudy compounds are close to the Seebeck

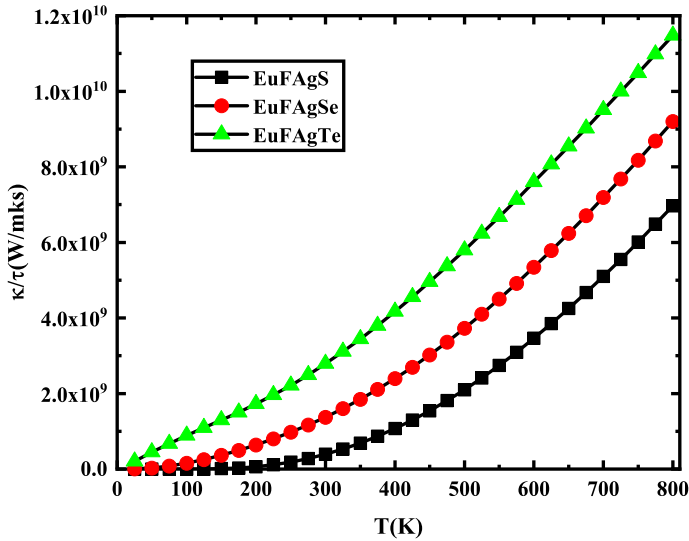


Fig. 8 Thermal conductivity of the layered structured EuFAGX (X = S, Se and Te) compounds

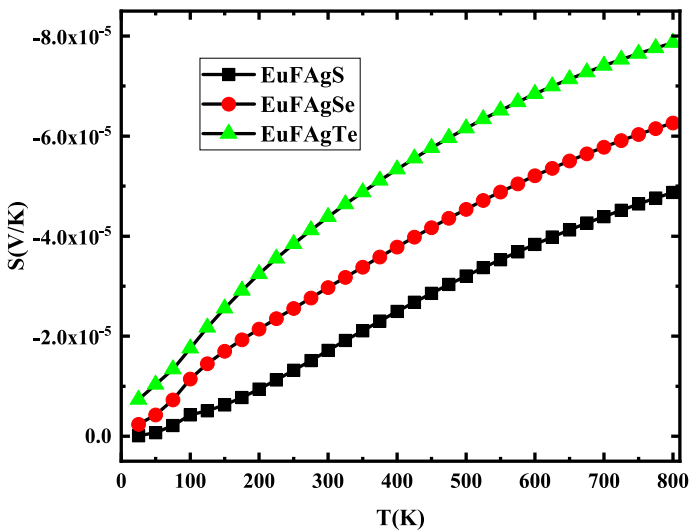


Fig. 9 Seebeck coefficient of the layered structured EuFAGX (X = S, Se and Te) compounds

value of Ba:BiCuSeO and BiCuOTe at room temperature make the reported results rational and logical.

A thermoelectric component called the power factor (PF) governs the power generation ability of materials. The calculated PF for these compounds is shown in Fig. 10; the PF of all compounds increases as the concentration of carriers grows with increasing temperature up to 300 K. The greatest value of PF for EuFAGX (X = S, Se and Te) compounds at 300 K temperature are 4.91×10^8 , 5.42×10^8 and 9.85×10^8 W/mK²s

respectively. The power factor of 0.35 mW/mK^2 was obtained for $\text{Bi}_{0.98}\text{Zn}_{0.02}\text{CuSeO}$ sample at 773 K, which is almost twice that of the pristine sample (0.18 mW/mK^2) at the same temperature. This value is lower than the Pb (0.8 mW/mK^2), Ba (0.62 mW/mK^2) and Ca (0.65 mW/mK^2) and for Mg (0.2 mW/mK^2) doped at Bi in BiCuSeO at 773 K (Zhao et al. 2014), for $\text{Bi}_{1-x}\text{Pb}_x\text{CuOTe}$ ($x=0, 0.01, 0.02, 0.04$ and 0.06) are $4\text{--}7.5 \times 10^{-4} \text{ W/mK}^2$, from 0.1 to $3.6 \text{ }\mu\text{W/cmK}^2$ (An et al. 2014), for $\text{Bi}_{1-x}\text{M}_x\text{CuSeO}$ ($M=\text{Mg, Ca, Sr, and Ba}$) at 300 K while 4.478 ($10^{10} \text{ W/mK}^2\text{s}$) and 5.949 ($10^{10} \text{ W/mK}^2\text{s}$) (Zhao et al. 2014) for SrFCuS and SrFCuSe , respectively at 600 K (Hoat 2019). The Power Factor of the understudy compound is reliable with the SrFCuS and SrFCuSe and are greater than the other reported results.

A unit less number called the figure of merit significantly impacts how well thermoelectric materials work. The figure of merit is the most crucial indicator of thermoelectric material performance. Figure 11 display the calculated ZT for each of these compounds; for EuFAgX ($X=\text{S, Se and Te}$) ZT values are $0.0176, 0.0394$ and 0.251 at room temperature and $0.263, 0.465$ and 0.807 at 800 K. The ZT value is 0.48 was achieved for the $\text{Bi}_{0.98}\text{Zn}_{0.02}$.

CuSeO sample at 773 K, Ni-doped BiCuSeO (0.25 at 773 K) for 0.04% and Mg-doped BiCuSeO (0.37 at 773 K) for 0.125% doping, 0.09 to 0.27 for $\text{Bi}_{1-x}\text{Pb}_x\text{CuOTe}$ ($x=0, 0.01, 0.02, 0.04$ and 0.06) at 300 K (An et al. 2014), and the ZT at 1200 K is 0.967 and 0.966 for SrFCuS and SrFCuSe respectively (Hoat 2019; Zhao et al. 2014). This high value of ZT for the understudy compounds makes them suitable for use in a variety of thermoelectric applications, consist of but not restricted to nano-thermocouples, thermoelectric peltier micro coolers, and thermoelectric power generators for wearable systems at low temperature (Din et al. 2022).

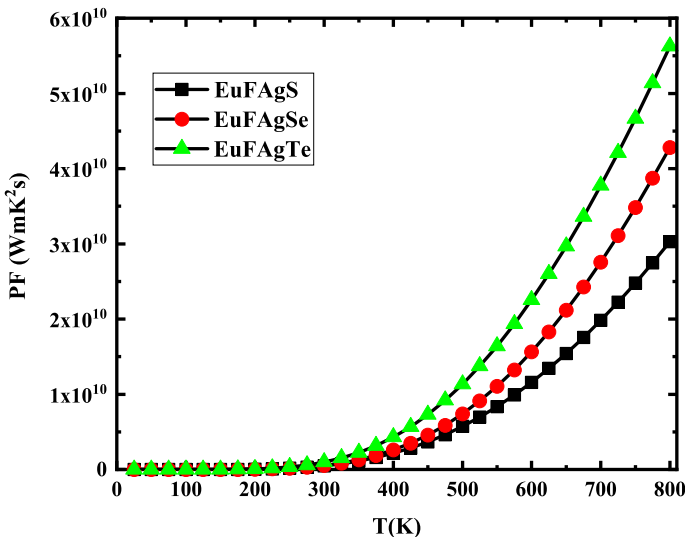


Fig. 10 Power Factor of the layered structured EuFAgX ($X=\text{S, Se and Te}$) compounds

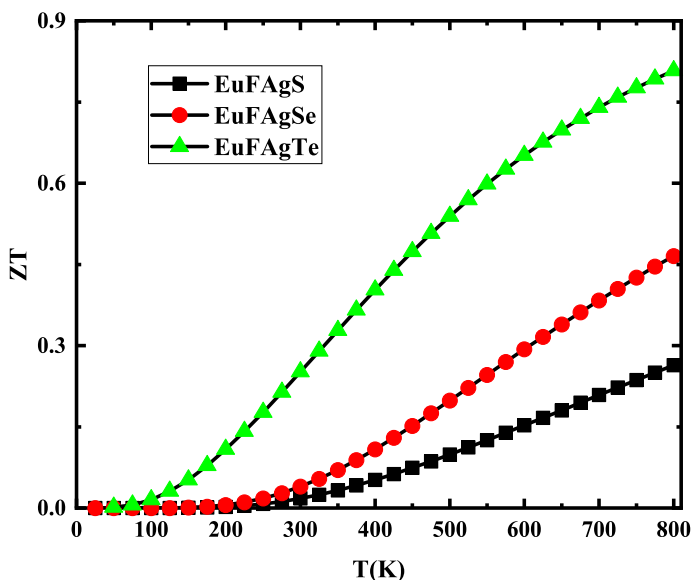


Fig. 11 ZT plot of the layered structured EuFAGX (X=S, Se and Te) compounds

3.5 Magnetic properties

Electron spin and orbital motion are intrinsically linked to the magnetic properties of materials.

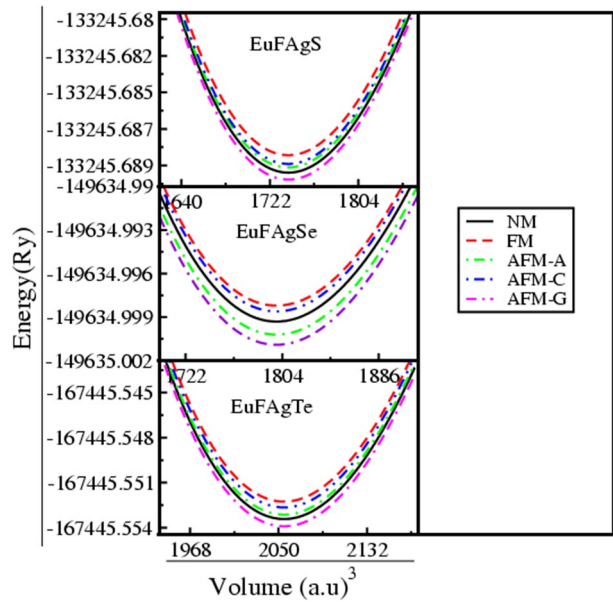
Magnetism in magnetic materials results from the exchange interactions of electrons. Materials are ferromagnetic when their magnetic moments align in a parallel fashion and they are anti-ferromagnetic when their magnetic moments are aligned anti-parallel (Kamioka et al. 2005; Boudiaf et al. 2018).

Figure 12 displays the magnetic ground state energy versus volume for ferromagnetic (FM), non-magnetic (NM) and A, C and G type anti-ferromagnetic (AFM) magnetic arrangements explored for studying the magnetic nature of EuFAGX (X=S, Se and Te). It can be seen from the figure that the G-type AFM is the stable magnetic phase for all compounds as its ground state energy is lower than that of the other magnetic phases. Similarly the isotropic Eu based EuTAsF.

(T=Zn, Mn, and Fe) compounds are also G-type AFM and AFM behavior is reported for EuMnPnF compounds (Pn=P, As, Sb) (Plokhikh et al. 2018).

The computed magnetic moments for Eu atom in EuFAGX (X=S, Se and Te) are presented in Table 2. The magnetic moments of Eu atom are 7.87, 7.69 and 7.56 μ_B respectively. Experimentally only magnetic moments for EuFAGSe and EuFAGTe are 7.78/Eu μ_B and 7.45/Eu μ_B respectively are reported (Plokhikh et al. 2020) and there is no data available for EuFAGS. On the other hand the magnetic moment per Eu is 7 μ_B and 7.67 μ_B for EuZnPnF (Pn=As, Sb), 5.47 μ_B , 4.59 μ_B and 5.64 μ_B for EuTAsF (T=Zn, Mn, and Fe) (Plokhikh et al. 2023). The calculated magnetic moment per Eu is in close agreement with the experiments and other reported results indicating that the reported results are reasonable. The magnetic moment of Eu atom is decreasing going from S to Te because of the distance between the Eu atom is increasing which decreases its transition temperature and magnetic moments (Alwadai et al. 2022; Asmar et al. 2018).

Fig. 12 magnetic optimization plot of the layered structured EuFAgX (X=S, Se and Te) compounds



The magnetic susceptibility (χ) for these EuFAgX (X=S, Se and Te) compounds is determined by BoltzTraP program (Koller et al. 2012) and explained through Curie Weiss law (Mehmood et al. 2020) represented in Fig. 13. The graph makes it evident that the understudy compounds are AFM in nature. The computed χ for EuFAgS is 1.31×10^{-3} emu/mole, for EuFAgSe is 1.32×10^{-3} emu/mole and for EuFAgTe is 1.34×10^{-3} emu/mole at 3 K. From the figure the transition temperatures (T_N) for these compounds are 10, 9 and

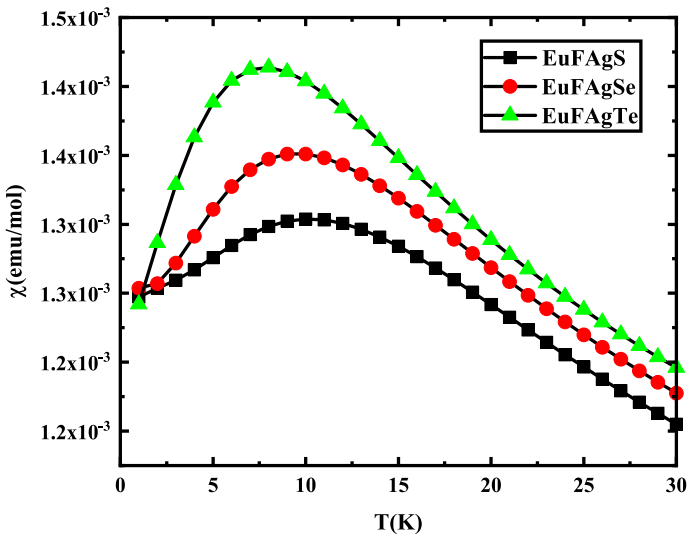


Fig. 13 Magnetic Susceptibility of the layered structured EuFAgX (X=S, Se and Te) compounds

8 K respectively for EuFAgX (X = S, Se and Te) compounds and experimentally reported T_N are 5 and 1.8 K for EuFAgX (X = S and Te). Similarly the T_N of 2 to 3 K and 2.4 to 3 K are reported for EuZnPnF (Pn = As, Sb) and EuTAsF (T = Zn, Mn, and Fe) (Plokhikh et al. 2023) make the results obtained for the understudy compounds are rational and logical. The outcomes for these compounds provided here are in good accord with the experimental data shows that the result reported for EuFAgSe is sensible. Conversely the χ for these compounds decreasing as progress from S to Te base compounds following the magnetic moments (Alwadai et al. 2022; Asmar et al. 2018). As the underlying compounds are anti-ferromagnetic, magnetic probes cannot access the information stored in anti-ferromagnetic moments. It is hence suitable for use in magnetically non-disruptive storage systems.

4 Conclusions

The FP-LAPW technique with GGA, GGA+U potentials with addition of, BJ+U and mBJ+U in the domain of DFT are utilized to examine the structural, optoelectronic thermoelectric and magnetic properties of EuFAgX (X = S, Se and Te) tetra one type compounds. All the structural parameters are in good approximation with experimental results. The result presented by total and partial density of state specify that EuFAgX (X = S, Se and Te) are semiconductor and their electrical conductivity also discloses the semiconductor nature of the corresponding compounds. 1.77–3.57 eV are the band gap values respectively for EuFAgX (X = S, Se and Te) and reduces as replacing S by se and Te and behave direct band gap nature elucidated from band structure. The outcomes demonstrate that under study materials are optically dynamic in the visible range of electromagnetic spectrum signifying that they could be employed suitable candidates for as solar cell device. The reported thermoelectric properties also suggest that these compounds are suitable materials for thermoelectric applications due to their anti-ferromagnetic nature these can be used as magnetic clocking devise as magnetic probes cannot access the information stored in anti-ferromagnetic moments and hence suitable for use in magnetically non-disruptive storage systems.

Author contributions HAS: Software, Formal analysis, Writing- Original draft preparation, Project administration. SM: Data curation, Methodology, Investigation, Writing- Reviewing and Editing; Supervision, Visualization Conceptualization.

Funding None.

Data availability The data used in the current study are available from the corresponding author on reasonable request.

Declarations

Conflict of interest The authors declare that they have no competing interest.

References

Abasi, T., Boochani, A., Masharian, S.R.: Metallic and intra-band investigation of optical properties for Borophene nano-sheet: a DFT study. *Int. Nano Lett.* **10**, 33–41 (2020)

- Al-Douri, Y., Merabet, B., Abid, H., Khenata, R.: First-principles calculations to investigate optical properties of $\text{ByAl}_x\text{In}_{1-x-y}\text{N}$ alloys for optoelectronic devices. *Superlattices. Microstruct.* **51**, 404 (2012)
- Aliabad, H.A.R., Hosseini, S.M., Kompany, A., Youssefi, A., Kakhki, E.A.: Optical properties of pure and transition metal-doped indium oxide. *Phys. Status Solidi B.* **246**, 1072 (2009)
- Almishal, S.S.I., Rashwan, O.: First-principles investigation of lead-free trigonal $\text{CsGeI}_{3-x}\text{Br}_x$ mixed-halide perovskite system for optoelectronic applications: electronic and optical properties. *Mater. Sci. Semicond. Process.* **151**, 107017 (2022)
- Alwadai, N., Mehmood, S., Ali, Z., Al-Buriah, M.S., Alomairy, S., Khosa, R.Y., Alrowaili, Z.A., Somaily, H.H., Aman, S., Farid, H.M.T.: Structural, electronic, elastic and magnetic properties of Ln_3QIn (Ln = Ce, Pr and Nd; Q = C and N) anti-perovskites. *J. Electro. Mater.* **51**, 2819–2827 (2022)
- An, T.H., Lim, Y.S., Choi, H.S., Seo, W.S., Park, C.H., Kim, G.R., Park, C., Lee, C.H., Shim, J.H.: Point defect-assisted doping mechanism and related thermoelectric transport properties in Pb-doped BiCuTe_2 . *J. Mater. Chem. A* **2**, 19759 (2014)
- Asmar, E., Tencé, S., Bobet, J.L., Ourane, B., Nakhli, M., Zakhour, M., Gaudin, E.: The Mg-Rich phase NdNiMg_{15} : structural and magnetic properties. *Inorg. Chem.* **57**, 14152–14158 (2018)
- Bannikov, V.V., Shein, I.R., Ivanovskii, A.L.: Design of novel magnetic materials based on ZrCuSiAs -like semiconducting pnictide-oxides from first-principles calculations. *Solid State Commun.* **150**, 2069–2071 (2010)
- Bannikov, V.V., Shein, I.R.I., A.: L, Electronic, optical properties and chemical bonding in six novel 1111-like chalcogenide fluorides AMChF (A = Sr, Ba; M = Cu, Ag; and Ch = S, Se, Te) from first principles calculations. *J. Solid State Chem.* **196**, 601–606 (2012a)
- Bannikov, V.V., Shein, I.R., Ivanovskii, A.L.: Structural, electronic properties and inter-atomic bonding in layered chalcogenide oxides LaMChO (M = Cu, Ag, and Ch = S, Se) from FLAPW-GGA calculations. *Solid State Sci.* **14**, 89–93 (2012b)
- Benahmed, A., Bouhemadou, A., Alqarni, B., Guechi, N., Al-Douri, Y., Khenata, R., Omran, S.B.: Structural, elastic, electronic, optical and thermoelectric properties of the Zintl-phase Ae_3AlAs_3 (Ae = Sr, Ba). *Philos. Mag.* **98**, 1217–1240 (2018)
- Birch, F.: Finite elastic strain of cubic crystals. *Phys. Rev.* **71**, 809–824 (1947)
- Blaha, P., Schwarz, K., Tran, F., Laskowski, R., Madsen, G., Mark, L.D.: WIEN2k: an augmented plane waves plus local orbitals program for calculating the properties of solid. *J. Chem. Phys.* **152**, 07410130 (2020)
- Bouafia, H., Sahli, B., Hiadi, S., Abidri, B., Rached, D., Akriche, A., Mesli, M.N.: Theoretical investigation of structural, elastic, electronic, and thermal properties of KCaF_3 , $\text{K}_{0.5}\text{Na}_{0.5}\text{CaF}_3$ and NaCaF_3 Perovskites. *Superlattice. Microst.* **82**, 525–537 (2015)
- Boudiaf, K., Bouhemadou, A., Boudrifra, O., Haddadi, K., Saoud, F.S., Khenata, R., Al-Douri, Y., Bin-Omran, S., Ghebouli, M.A.: Structural, elastic, electronic and optical properties of LaOAgS -type silver fluoride chalcogenides: first-principles study. *J. Electron. Mater.* **46**, 4539–4556 (2017a)
- Boudiaf, K., Bouhemadou, A., Boudrifra, O., Haddadi, K., Saoud, F.S., Khenata, R., Al-douri, Y., Omran, S.B., Ghebouli, M.A.: Structural, elastic, electronic and optical properties of LaOAgS -type silver fluoride chalcogenides: first-principles study. *J. Electron. Mater.* **46**, 4539–4556 (2017b)
- Boudiaf, K., Bouhemadou, A., Khenata, R., Al-Douri, Y., Bin-Omran, S., Ghebouli, M.A.: Electronic and thermoelectric properties of the layered BaFAgCh (Ch = S, Se and Te): First-principles study. *J. Alloys Compd.* **759**, 32–43 (2018)
- Charkin, D.O., Urmanov, A.V., Kazakov, S.M.: Preparation and crystal structures of novel LaOAgS -type copper and silver fluoride chalcogenides. *J. Alloys Compd.* **516**, 134–138 (2012)
- Charkin, D.O., Urmanov, A.V., Plokhikh, I.V., Korshunov, A.D., Kuznetsov, A.N., Kazakov, S.M.: Synthesis and crystal structures of novel LaOAgS -type alkaline earth-zinc, manganese, and cadmium fluoride pnictides. *J. Alloys Compd.* **585**, 644–649 (2014)
- Chaudhry, A.R., Ahmed, R., Irfan, A., Mohamad, M., Muhammad, S., Haq, B.U., Abdullah Al-Sehemi, G.: Al-Douri Y Optoelectronic properties of naphtho[2, 1-b:6, 5-b']difuran derivatives for photovoltaic application: a computational study. *J. Mol. Model.* **22**, 1–13 (2016)
- Das, S., Ramakrishnan, A., Rudra, M., Chen, K., Sinha, T.P., Misra, D.K., Mallik, R.C.: Thermoelectric properties of Zn Doped BiCuSeO . *J. Electron. Mater.* **48**, 3631–3642 (2019)
- Din, M.U., Ain, Q., Yousaf, M., Munir, J.: Structural, elastic, electronic, optical and thermoelectric response of lead-free double perovskite $\text{Rb}_2\text{TlInX}_6$ (X = Cl, I) for energy storage devices: DFT+SOC investigations. *Mater. Sci. Semicond. Process.* **152**, 107081 (2022)
- Elqahtani, Z.M., Aman, S., Mehmood, S., Ali, Z., Hussanan, A., Ahmad, N., Alomairy, S., Al Buriah, M.S., Alrowaili Z.A., Farid, H.M.T.: n-Type narrow band gap A InAs (A = Sr and Eu) Zintl phase semiconductors for optoelectronic and thermoelectric applications. *J. Taibah Uni. Sci.* **16**, 660–669 (2020)

- Gamon, J., Giaume, D., Wallez, G., Labégorre, J.B., Lebedev, O.I., Orabi, R.A., Haller, S., Mercier, T.L., Guilmeau, E., Maignan, A., Barboux, P.: Substituting copper with silver in the BiMOCh layered compounds (M = Cu or Ag; Ch = S, Se, or Te): crystal, electronic structure, and optoelectronic properties. *Chem. Mater.* **30**(2), 549–558 (2018)
- Gerke, B., Schwickert, C., Stoyko, S.S., Khatun, M., Mar, A., Pöttgen, R.: Magnetic hyperfinefield splitting in EuAg₄As₂ and EuAg₄Sb₂. *Solid State Sci.* **20**, 65 (2013)
- Gudelli, V.K., Kanchana, V., Vaitheswaran, G., Singh, D.J., Svane, A., Christensen, N.E., Mahanti, S.D.: Electronic structure, transport, and phonons of SrAgChF (Ch = S, Se, Te): bulk superlattice thermoelectrics. *Phys. Rev. B* **92**, 045206 (2015)
- Hiramatsu, H., Ueda, K., Ohta, H., Kamiya, T., Hirano, M., Kikuchi, M., Yanagi, H., Kamiya, T., Hosono, H.: Heavy hole doping of epitaxial thin films of a wide gap p-type semiconductor, LaCuOSe, and analysis of the effective mass. *Appl. Phys. Lett.* **91**, 012104 (2007)
- Hiramatsu, H., Yanagi, H., Kamiya, T., Ueda, K., Hirano, M., Hosono, H.: Crystal structures, optoelectronic properties, and electronic structures of layered oxychalcogenides MCuOCh (M = Bi, La; Ch = S, Se, Te): effects of electronic configurations of M³⁺ ions. *Chem. Mater.* **20**, 326–334 (2008)
- Hoat, D.M.: Theoretical investigations on physical properties of SrFCuCh (Ch = S and Se). *J. Solid State Chem.* **271**, 191–198 (2019)
- Hoat, D.M., Silva, J.F.R., Blas, A.M.: Systematic study of structural, electronic, optical and thermodynamic properties of SrFCuTe compound. *J. Solid State Chem.* **270**, 85–91 (2019)
- Hohenberg, P., Kohn, W.: Inhomogeneous electron gas. *Phys. Rev. B* **136**, 864 (1964)
- Hu, D.Y., Zhao, X.H., Tang, T.Y.Lu., Li, L.M., Gao, L., Tang, L.K., Y. L.: Study on the structural, electronic and optical properties of double-perovskite halides Cs₂AgSbX₆ (X=I, Br, Cl) based on first-principles. *Mater. Sci. Semicond. Process.* **152**, 107077 (2022)
- Johnston, D.C.: The puzzle of high temperature superconductivity in layered iron pnictides and chalcogenides. *Adv. Phys.* **59**, 803 (2010)
- Kamihara, Y., Watanabe, T., Hirano, M., Hosono, H.: Iron-Based Layered Superconductor LaO F FeAs (x = 0.05–0.12) with T_c = 26 K. *J. Am. Chem. Soc.* **130**, 3296 (2008)
- Kamioka, H., Hiramatsu, H., Hirano, M., Ueda, K., Kamiya, T., Hosono, H.: Excitonic properties related to valence band levels split by spin-orbit interaction in layered oxychalcogenide LaCuOCh(Ch=S,Se). *J. Lumin.* **112**, 66 (2005)
- Khan, S., Mehmood, N., Ahmad, R., Kalsoom, A., Hameed, K.: Analysis of structural, elastic and optoelectronic properties of indium-based halide perovskites InACl₃ (A = Ge, Sn, Pb) using density functional theory. *Mater. Sci. Semicond. Process.* **150**, 106973 (2022)
- Kohn, W., Sham, L.J.: Self-consistent equations including exchange and correlation effects. *Phys. Rev.* **140**, A1133 (1965)
- Koller, D., Tran, F., Blaha, P.: Improving the modified Becke-Johnson exchange potential. *Phys. Rev. B* **85**, 155109 (2012)
- Lin, D., Luo, Q., Zheng, H., Tang, L., Zhan, W., Tang, K.: A new oxygen-free cobalt-based compound SmCoAsF with multiple magnetic transitions. *Cryst. Eng. Comm.* **22**, 4268–4274 (2020)
- Liu, G., Sun, H., Zhou, J., Li, Q., Wan, X.G.: Thermal properties of layered oxychalcogenides BiCuOCh (Ch = S, Se, and Te): a first-principles calculation. *J. Appl. Phys.* **119**, 185109e1 (2016)
- Loughin, S., French, R.H., Noyer, L.K., Ching, W.Y., Xu, Y.N.: Critical point analysis of the interband transition strength of electrons. *J. Phys. D.* **29**, 1740 (1996)
- Madsen, G.K.H., Sing, D.J., BoltzTrape: A code for calculations band structure dependent Quantities. *Comput. Phys. Commun.* **175**(1), 6771 (2006)
- Mehmood, S., Ali, Z., Khan, I., Ahmad, I.: Effects of Ni substitution on the electronic structure and magnetic properties of perovskite SrFeO₃. *J. Electron. Mater.* **49**(6), 3780–3790 (2020)
- Motomitsu, E., Yanagi, H., Kamiya, T., Hirano, M., Hosono, H.: Synthesis, structure and physical properties of layered semiconductors MCuFCh (M = Sr, Eu, Ch = S, Se). *J. Solid State Chem.* **179**, 1668 (2006)
- Mukherjee, M., Singh, A.K.: Strong chemical bond hierarchy leading to exceptionally high thermoelectric figure of merit in oxychalcogenide AgBiTeO. *ACS Appl. Mater. Interfaces* **12**, 8280–8287 (2020). <https://doi.org/10.1021/acsami.9b21358>
- Park, C.H., Kykyneshi, R., Yokochi, A., Tate, J., Keszler, D.A.: Structure and physical properties of BaCuTeF. *J. Solid State Chem.* **180**, 1672–1677 (2007)
- Patschke, R., Brazis, P., Kanneur, C.R., Kanatzidis, M.G.: Cu_{0.66}EuTe₂, KCu₂EuTe₄ and Na_{0.2}Ag_{2.8}EuTe₄: compounds with modulated square Te nets. *J. Mater. Chem.* **9**, 2293 (1999)
- Penn, D.R.: Wave-number-dependent dielectric function of semiconductors. *Phys. Rev.* **128**(5), 2093 (1962)
- Perdew, J.P., Burke, K., Wang, Y.: Generalized gradient approximation for the exchange-correlation hole of a many-electron system. *Phys. Rev. Lett.* **54**, 16533 (1996)

- Plokhikh, I.V., Charkin, D.O., Verchenko, V.Y., Kuznetsov, A.N., Kazakov, S.M., Tsirlin, A.A., Shevelkov, A.V.: Structural and thermodynamic stability of the “1111” structure type: a case study of the EuFZnPn series. *Inorg. Chem.* **55**, 12409 (2016)
- Plokhikh, I.V., Charkin, D.O., Verchenko, V.Y., Kuznetsov, A.N., Kazakov, S.M., Tsirlin, A.A., Shevelkov, A.V.: Synthesis, crystal structure and physical properties of europium-manganese fluoride pnictides, EuMnPnF (Pn = P, As, Sb). *J. Solid State Chem.* **258**, 682 (2018)
- Plokhikh, I.V., Kuznetsov, A.N., Charkin, D.O., Shevelkov, A.V., Pfitzner, A.: Layered compounds BaFMgPn(Pn = P, As, Sb, and Bi), transition-metal-free representatives of the 1111 structure type. *Inorg. Chem.* **58**, 3435 (2019)
- Plokhikh, I.V., Tsirlin, A.A., Heletta, L., Klenner, S., Charkin, D.O., Kuznetsov, A.N., Shevelkov, A.V., Pöttgen, R., Pfitzner, A.: Synthesis, electronic structure and physical properties of two new layered compounds, EuFAgSe and EuFAg₁₋₅Te, featuring the active redox pair Eu²⁺/Ag⁺. *Dalton Trans.* **49**, 7426–7435 (2020)
- Plokhikh, I.V., Tsirlin, A.A., Khalyavin, D.D., Fischer, H.E., Shevelkov, A.V., Pfitzner, A.: Effect of antiferroite layer on the magnetic order in Eu-based 1111 compounds, EuTAsF (T = Zn, Mn, and Fe). *Phys. Chem. Chem. Phys.* **25**, 4862–4871 (2023)
- Pöttgen, R., Johrendt, D.: Materials with ZrCuSiAs-type structure, *Z. Naturforsch. B. Chem. Sci.* **63**, 1135–1148 (2008)
- Qaisi, S.A., Mushtaq, M., Alomairy, S., Vu, T.V., Rached, H., Haq, B.U., Mahmood, Q., Buriahi, M.S.A.: First-principles investigations of Na₂CuMCl₆ (M = Bi, Sb) double perovskite semiconductors: Materials for green technology. *Mater. Sci. Semicond. Process.* **150**, 106947 (2022)
- Rehman, J., Usman, M., Tahir, M.B., Hussain, A., Rehman, M.A., Ahmad, N., Muhammad, S.: First-principles calculations to investigate structural, electronic and optical properties of Na based fluoroperovskites NaXF₃ (X = Sr, Zn). *Solid State Commun.* **2021**, 114396 (2021)
- Rehman, M.Z., Shaimaa, A.M., Abdelmohsen Eman, A., Mahmoud, M., Saeed, U., Idress, M., Shafiq, M., Amin, B., Saeed, Y.: First principles study of structural electronic elastic and optical properties of Cs₂LiTiBr₆ and Cs₂NaTiBr₆. *Mater. Sci. Semicond. Process.* **151**, 106993 (2022)
- Richard, A.P., Russell, J.A., Zakutayev, A., Zakharov, L.N., Keszler, D.A., Tate, J.: Synthesis, structure, and optical properties of BiCuOCh (Ch = S, Se, and Te). *J. Solid State Chem.* **187**, 15–19 (2012)
- Salik, L., Bouhemadou, A., Boudiaf, K., Saoud, F.S., Omran, S.B., Khenata, R., Al-Douri, Y., Reshak, A.H.: Structural, elastic, electronic, magnetic, optical, and thermoelectric properties of the diamond-like quaternary semiconductor CuMn₂InSe₄. *J. Supercond. Nov. Magn.* **33**, 1091–1102 (2020)
- Saparov, B., Singh, D.J., Garlea, V.O., Sefat, A.S.: Crystal, magnetic, and electronic structures, and properties of new BaMnPnF (Pn = As, Sb, Bi). *Sci. Rep.* **3**, 2154 (2013)
- Selmani, Y., Labrim, H., Moutassime, A., Bahmad, L.: Structural, optoelectronic and thermoelectric properties of Cs-based fluoroperovskites CsMF₃ (M = Ge, Sn or Pb). *Mater. Sci. Semicond. Process.* **152**, 107053 (2022)
- Shahzad, M., Hussain, S., Farooq, M.U., Laghari, R.A., Bilal, M.H., Khan, S.A., Tahir, M.B., Khalil, A., Rehman, J.U., Ali, M.M.: First-principles calculations to investigate structural, electronic, elastic and optical properties of radium based cubic fluoro-perovskite materials. *Heliyon* **9**, e13687 (2023)
- Shannon, R.D.: Revised effective ionic radii and systematic studies of interatomic distances in halides and chalcogenides. *Acta Crystallogr.* **32**, 751 (1976)
- Sharma, N., Chandra, D., Rathi, A., Singh, A.K.: First-principles WC-GGA and mBJ calculations for structural, electronic, optical and elastic properties of M_xGa_{1-x}Sb (M = Al, In, B) ternary alloys. *Mater. Sci. Semicond. Process.* **151**, 107033 (2022)
- Su, Y., Wang, H., Shi, L.B., Wang, Y.Z., Liu, Q., Qian, P.: An investigation on carrier transport behavior of tetragonal halide perovskite: first-principles calculation. *Mater. Sci. Semicond. Process.* **151**, 103836 (2022)
- Taha, T.A., Mehmood, S., Ali, Z., Khan, S.R., Aman, S., Farid, H.M.T., Trukhanov, S.V., Zubar, T.I., Tishkevich, D.I., Trukhanov, A.V.: Structure, Magnetic, Opto-electronic and thermoelectric properties of A₃In₂As₄ and A₅In₂As₆ (A = Sr and Eu) Zintl phase compounds. *J. Alloys Compound.* **938**, 168614 (2023)
- Tran, F., Blaha, P.: Accurate Band Gaps of Semiconductors and Insulators with a Semilocal Exchange-Correlation Potential. *Phys. Rev. Lett.* **102**, 226401 (2009)
- Tsuneda, T., Hirao, K.: Self-interaction corrections in density functional theory. *J. Chem. Phys.* **140**(18), 18A5131 (2014)
- Ueda, K., Hiramatsu, H., Ohta, H., Hirano, M., Kamiya, T., Hosono, H.: Optoelectronic properties and electronic structure of YCuOSe. *Phys. Rev. B* **69**, 55305 (2004)

- Ul Islam, A.K.F., Helal, M.A., Liton, M.N.H., Kamruzzaman, M., Islam, H.M.T.: First principles study of electronic structure dependent optical properties of oxychalcogenides BiOCuCh (Ch = S, Se, Te), Indian. J. Phys. **91**, 403–412 (2017)
- Ullah, I., Murtaza, G., Khenata, R., Mahmood, A., Yar, A., Muzammil, M., Amin, N., Seleh, M.: Structural and Optoelectronic Properties of X_2Zn (X = Ca, Sr, Ba; Z = As, Sb, Bi) Anti-Perovskite Compounds. J. Electro. Mater. **45**, 3059–3068 (2016)
- Wager, J.F., Keszler, D.A., Presley, R.E.: Transparent Electronics. Springer, Berlin (2008)
- Yanagi, H., Tate, J., Park, S., Park, C.H., Keszler, D.A.: P-type conductivity in wideband-gap BaCuQF (Q = S, Se). Appl. Phys. Lett. **82**, 2814e1 (2003)
- Yanagi, H., Tate, J., Park, S., Park, C., Keszler, D.A., Hirano, M., Hosono, H.: Valence band structure of BaCuSF and BaCuSeF. J. Appl. Phys. **100**, 083705e1 (2006)
- Yasukawa, M., Ueda, K., Hosono, H.: Thermoelectric properties of layered oxyselenides La $_{1-x}$ Sr $_x$ CuOSe (x = 0 to 0.2). J. Appl. Phys. **95**, 3594–3597 (2004)
- Zakutayev, A., Tate, J., Platt, H.A.S., Keszler, D.A., Hein, C., Mayer, T., Klein, A.W.: Jaegermann, Electronic properties of BaCuChF (Ch = S, Se, Te) surfaces and BaCuSeF/ZnTe interfaces. J. Appl. Phys. **107**, 103713-1–103718 (2010a)
- Zakutayev, A., Tate, J., Schneider, G.: Defect physics of BaCuChF (Ch = S, Se, Te) p-type transparent conductors. Phys. Rev. B **82**, 195204 (2010b)
- Zakutayev, A., Kykyneshi, R., Schneider, G., McIntyre, D.H., Tate, J.: Electronic structure and excitonic absorption in BaCuChF (Ch = S, Se, and Te). Phys. Rev. B **81**, 155103 (2010c)
- Zakutayev, A., Tate, J., Xie, S., Gibbons, B.J., Platt, H.A.S., Keszler, D.A., Barati, A., Klein, A., Jaegermann, W.: Interdiffusion at the BaCuSeF/ZnTe interface. Thin Solid Films **2011**, 7369–7373 (2011)
- Zhao, L.D., He, J., Berardan, D., Lin, Y., Li, J.F., Nan, C.W., Dragoe, N.: BiCuSeO oxyselenides: new promising thermoelectric materials. Energy Environ. Sci. **7**, 2900–2924 (2014)
- Zou, D., Xie, S., Liu, Y., Lin, J., Li, J.: Electronic structures and thermoelectric properties of layered BiCuOCh oxychalcogenides (Ch = S, Se and Te): first principles calculations. J. Mater. Chem. A **1**, 8888–8896 (2013)
- Zou, D., Zheng, H., Li, J.: Predicted thermoelectric properties of natural superlattice structural compounds BaCuChF (Ch = S, Se and Te) by first-principles calculations. J. Alloys Compd. **686**, 571–576 (2016)

Publisher's Note Springer Nature remains neutral with regard to jurisdictional claims in published maps and institutional affiliations.

Springer Nature or its licensor (e.g. a society or other partner) holds exclusive rights to this article under a publishing agreement with the author(s) or other rightsholder(s); author self-archiving of the accepted manuscript version of this article is solely governed by the terms of such publishing agreement and applicable law.